Spot-scanning beam delivery with laterally- and longitudinally-mixed spot size pencil beams in heavy ion radiotherapy *

Yuan-Lin Yan(闫渊林)[1,2,3,4] Xin-Guo Liu(刘新国)[1,2,3] Zhong-Ying Dai(戴中颖)[1,2,3]
Yuan-Yuan Ma(马圆圆)[1,2,3,4] Peng-Bo He(贺鹏博)[1,2,3] Guo-Sheng Shen(申国盛)[1,2,3,4]
Teng-Fei Ji(姬腾飞)[1,2,3,4] Hui Zhang(张晖)[1,2,3,4] Qiang Li(李强)[1,2,3;1)]

[1] Institute of Modern Physics, Chinese Academy of Sciences, Lanzhou 730000, China
[2] Key Laboratory of Heavy Ion Radiation Biology and Medicine of Chinese Academy of Sciences, Lanzhou 730000, China
[3] Key Laboratory of Basic Research on Heavy Ion Radiation Application in Medicine, Gansu Province, Lanzhou 730000, China
[4] University of Chinese Academy of Sciences, Beijing 100049, China

Abstract: The three-dimensional (3D) spot-scanning method is one of the most commonly used irradiation methods in charged particle beam radiotherapy. Generally, spot-scanning beam delivery utilizes the same size pencil beam to irradiate the tumor targets. Here we propose a spot-scanning beam delivery method with laterally- and longitudinally-mixed size pencil beams for heavy ion radiotherapy. This uses pencil beams with a bigger spot size in the lateral direction and wider mini spread-out Bragg peak (mini-SOBP) to irradiate the inner part of a target volume, and pencil beams with a smaller spot size in the lateral direction and narrower mini-SOBP to irradiate the peripheral part of the target volume. Instead of being controlled by the accelerator, the lateral size of the pencil beam was adjusted by inserting Ta scatterers in the beam delivery line. The longitudinal size of the pencil beam (i.e. the width of the mini-SOBP) was adjusted by tilting mini ridge filters along the beam direction. The new spot-scanning beam delivery using carbon ions was investigated theoretically and compared with traditional spot-scanning beam delivery. Our results show that the new spot-scanning beam delivery has smaller lateral penumbra, steeper distal dose fall-off and the dose homogeneity (1-standard deviation/mean) in the target volume is better than 95%.

Keywords: heavy ion radiotherapy, spot-scanning, beam spot size, mini spread-out Bragg peak (mini-SOBP), mini ridge filter (mini-RF)

PACS: 87.53.Kn, 87.55.K-, 87.56.bd **DOI:** 10.1088/1674-1137/41/9/098201

1 Introduction

Beam scanning in charged particle therapy irradiates a target volume three dimensionally through lateral beam deflection by a pair of orthogonal dipole magnets in combination with longitudinal beam energy variation. The best known transverse beam scanning techniques are spot-scanning [1], raster scanning [2], and continuous raster scanning [3]. Depth beam scanning can be realized through active energy variation by a synchrotron, passive range shifter, and newly-developed hybrid method [4]. In the Heavy Ion Research Facility in Lanzhou (HIRFL) at the Institute of Modern Physics (IMP), Chinese Academy of Sciences, active scanned beam delivery has already been realized and tested, using the spot-scanning technique with beam energy variation by a synchrotron [5, 6]. In the heavy ion spot-scanning technique, the Bragg peaks are superposed to form a homogeneous dose distribution in the longitudinal direction. Because the original Bragg peak is too sharp, heavy ion radiotherapy needs a large number of iso-energy layers. Therefore, mini ridge filters (mini-RFs) are used in spot-scanning beam delivery to widen the original Bragg peak to a mini spread-out Bragg peak (mini-SOBP) and reduce the number of iso-energy layers. At each iso-energy layer, the beam is delivered as a series of discrete points to the target volume. Once the particle count reaches the required value for each scan point, the beam supply is switched off and then the pencil beam position is deflected to the next point by the scanning dipole magnets. Inevitably, unwanted particles are delivered to the pre-defined scan points due to the beam-off time delay.

Received 11 November 2016, Revised 23 April 2017

∗ Supported by Key Project of National Natural Science Foundation of China (U1232207), National Key Technology Support Program of the Ministry of Science and Technology of China (2015BAI01B11), National Key Research and Development Program of the Ministry of Science and Technology of China (2016YFC0904602) and National Natural Science Foundation of China (11075191, 11205217, 11475231, 11505249)

1) E-mail: liqiang@impcas.ac.cn

©2017 Chinese Physical Society and the Institute of High Energy Physics of the Chinese Academy of Sciences and the Institute of Modern Physics of the Chinese Academy of Sciences and IOP Publishing Ltd

So Inaniwa et al. integrated the extra dose due to the time delay into the weighting matrix optimization [7], and the accelerator was controlled rapidly to achieve a fast beam-off operation [8, 9].

Small size beam spots are usually desired for 3D spot-scanning beam delivery because the resulting steep lateral dose profile can avoid radiation damage to the healthy tissue surrounding a target volume to the maximum extent. However, spot-scanning beam delivery using small beam spot sizes means an enormous number of scanned points, which then requires higher accuracy of the beam exposure parameters. Kang et al. proposed that utilizing mixed size beam spots in a single treatment plan can solve the contradiction mentioned above [10]. Simultaneously, short distal dose fall-off distances (i.e. high distal dose fall-off gradients) are needed in the 3D spot-scanning beam delivery in order to furthest reduce the damage to the healthy tissue and OAR behind a target volume, which requires narrow mini-SOBPs for longitudinal dose superposition, thereby prolonging the treatment time. In layer-stacking conformal heavy-ion therapy based on a passive beam delivery system, wide mini-SOBPs were employed in the proximal and central parts of a SOBP while narrow mini-SOBPs were used in the distal end of the SOBP to reduce damage to the healthy tissue and OAR behind the tumor [11]. This paper proposes an active spot-scanning delivery method using two lateral and longitudinal sizes of pencil beams to solve the contradiction of pencil beam spot sizes as well as the contradiction of longitudinal width of mini-SOBPs. The pencil beam lateral size can be adjusted by precise accelerator control; however, this is a time-consuming process during the commissioning period of the accelerator and demands more advanced accelerator technologies. In the present study, the lateral spot size of a pencil beam was changed by inserting Ta scatterers. Mini-SOBPs with different full widths at the half maximum (FWHMs) can be generated using two different mini-RFs [11]. For passive proton beam delivery, Nakagawa et al. suggested that different widths of SOBP could be obtained through tilting a ridge filter [12]. In this paper, the longitudinal width of the mini-SOBP was changed by tilting a mini-RF. In addition, the new method was investigated theoretically for spot-scanning beam delivery with laterally- and longitudinally-mixed spot size pencil beams of carbon ions.

2 Materials and methods

2.1 Accelerator model and spot-scanning beam delivery used in this study

A hospital-based carbon ion therapy facility, the Heavy Ion Medical Machine (HIMM), is now under commissioning in Wuwei, China, and will start operation for tumor treatment in 2017.The compact HIMM facility consists of a synchrotron as the main accelerator, a cyclotron as the injector, and four treatment rooms [13, 14]. The beam intensity supplied by the HIMM facility can be selected from 2×10^6 to 4×10^8 particles per spill (pps).

In the spot-scanning beam delivery supposed in this study, the pencil beam is blocked when shifting the beam from one scan point to the next. A beam-off signal is sent to the beam stopper through the interlock control system once the scan point has already been irradiated with the required particles. However, the beam cutoff will be delayed by a few hundreds of microseconds (0.5 ms was supposed in this study) after the beam monitor sends a beam-off signal. Hence, each scan point is irradiated with some unwanted particles. Actually, the interlock control system sends the beam-off signal to the beam stopper in advance in order to eliminate the redundant particles caused by the beam-off delay. That is, the interlock control system gives the beam cutoff signal to the stopper when the monitor count has not yet reached the preset count for each scan point. The difference between the preset count and the measured count of the monitor when the beam control system sends the beam-off signal is described as the threshold. The calibration factor between the particle number and monitor count is related to the beam energy and the beam monitor. This study just considers the particle number threshold, which is the difference between the numbers of particles pre-defined and delivered when the beam-off signal is sent.

2.2 Monte Carlo simulation

In this study, a Monte Carlo (MC) method was used to simulate the beam transport in the supposed spot-scanning beam delivery system. The MC code SHIELD-HIT12A [15–17], which precisely simulates therapeutic beams of protons and ions in biological tissues relevant for particle therapy, is capable of transporting hadrons including nucleons, any ions, pions, antiprotons and antineutrons.

As shown in Fig. 1, the supposed spot-scanning beam delivery system consists of a pair of orthogonal dipole magnets, main and subdose monitors, a position monitor and a mini-RF. The iso-center of the treatment room is 1.05 m away from the vacuum window of the accelerator. This configuration is the same as that at HIRFL [18].The structure period of the mini-RF was 2 mm. In the MC simulations, carbon ion beams with different energies were focused at the iso-center to form Gaussian-shaped beam spots. The sampled number was 5×10^6 and the statistical accuracy was 1 mm, 1 mm and 0.1 mm in the x, y, and z directions respectively. Basic data of the pencil carbonion beams were calculated with the SHIELD-HIT12A code, including the ranges, depth-dose distributions and depth-beam spot size (σ) distributions

of 10 discrete energies from 180 MeV/u to 360 MeV/u in water. The basic data of the other energy carbon-ion beams not mentioned above were obtained by interpolation.

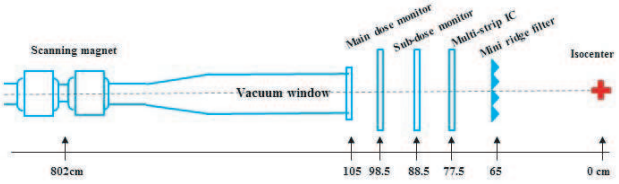

Fig. 1. (color online) Sketch diagram of the nozzle and components.

2.3 Varying pencil beams laterally and longitudinally

In this study, we applied scatterers of different thicknesses to the spot-scanning beam delivery system to enlarge the lateral size of beam spot slightly. Generally, materials like lead (Pb) and tantalum (Ta) are used as scatterers in passive beam delivery systems in order to obtain an irradiation field homogeneous and big enough for heavy ions [19, 20]. Because of its stronger scattering effect, tantalum was chosen as the scatterer. It was inserted 104.5 cm away from the iso-center of the treatment room, which is between the vacuum window and the main dose monitor. To enlarge beam spots with σ 3 mm to beam spots with σ 5 mm, the thicknesses of the tantalum scatterer for pencil carbonion beams with different energies were calculated.

Mini-RFs [11, 21], also called ripple filters [22], widen a Bragg peak to a Gaussian peak, a socalled mini-SOBP, to reduce the slice number and smooth the dose distribution across the target volume in spot-scanning beam delivery. The full height of the mini-RF is correlated with the width of the resulting mini-SOBP. Each width of the stairs corresponds to beam intensity or beam weight, while each height of the stairs represents decreased beam energy. The path length for which the beam passes through the mini-RF changes from $h(x,y)$ to $h(x,y)/\cos\theta$ when tilting the mini-RF from 0 to θ degrees as shown in Fig. 2, where (x, y) means the beam position in the beam coordinate system. After tilting the mini-RF, the step heights of the stairs will be enlarged to form a wider mini-SOBP longitudinally while the beam weight of each step remain unchanged. In fact, tilting mini-RF also broadens the lateral size of the beam spots. Because mini-RFs are usually made of aluminum, the lateral broadening effect on beam spots is small. In the MC simulation, tilting the mini-RF was simplified by replacing the original data of the ridge height from h to $h/\cos\theta$, owing to the SHIELD-HIT12A code being unable to process the spatial transforms of geometries. This approximation is proper because the scanning angles are small and its effect on oblique incidence is small. A mini-RF with FWHM of 8 mm for a carbon ion beam, designed and used at IMP, was made of aluminum and used in this study. Tilting the mini-RF 0°, 30°, 45° and 60° was simulated and the enlargement effects longitudinally (mini-SOBP) as well as laterally (beam spot size) were calculated.

2.4 Proposed spot-scanning beam delivery with laterally- and longitudinally-mixed size pencil beams

The principle of our proposed spot-scanning beam delivery with laterally- and longitudinally-mixed size pencil beams is shown schematically in Fig. 3. Large spot pencil beams broadened by the scatterer were used to irradiate the inner part of a target volume, while the original small pencil beams were employed to irradiate the peripheral part of the target volume. Meanwhile, the

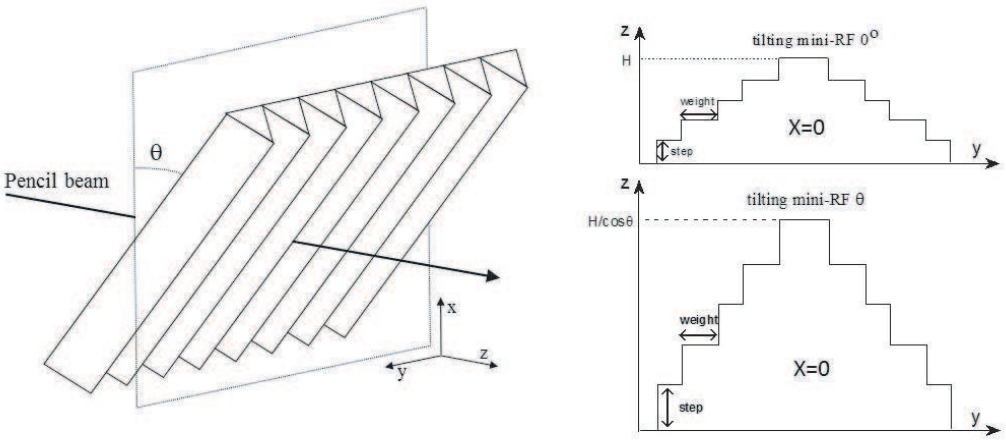

Fig. 2. Sketch diagram of tilting a mini-RF.

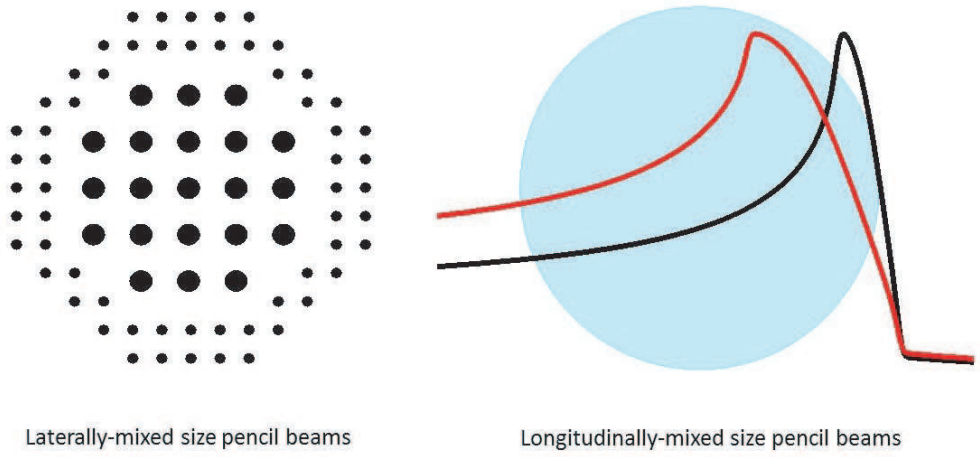

Fig. 3. (color online) Principle of spot-scanning beam delivery with laterally- and longitudinally-mixed size pencil beams.

distal end of the target volume was irradiated with the original mini-SOBP while the other part of the target volume in depth was irradiated with widened mini-SOBPs by means of tilting the mini-RF with appropriate angles. In this study, a virtual spherical target volume with diameter of 6 cm was assumed, located at depths from 7 to 13 cm in a water phantom. A pencil carbon-ion beam with spot size (σ) of 5 mm and mini-SOBP of 16 mm FWHM was taken as the large size beam a pencil carbon-ion beam with spot size (σ) of 3 mm and mini-SOBP of 8 mm FWHM as the small size one. The spot-scanning technique with laterally- and longitudinally-mixed size pencil beams is different from the only laterally-mixed size spot-scanning beam delivery described in the work by Kang et al [10]. For comparison, spot-scanning beam deliveries with the proposed laterally- and longitudinally-mixed size beam spots, single large size beams and single small size beams were used to irradiate the same target volume. The physical dose distributions optimized for the three mode beam deliveries above in terms of lateral penumbra, dose distal fall-off distance and homogeneity in the target volume were compared. The dose optimization procedure is described below.

Kraemer et al. showed that taking no more than 1/3 of the spot FWHM (i.e. 2.355/3 of σ) as the scanning step can achieve a sufficiently homogeneous dose distribution [23]. For the large size pencil beam with 5 mm σ spot size and 16 mm FWHM mini-SOBP, scan step sizes in the x, y and z directions were all selected as 4 mm. For the small size pencil beam with 3 mm sigma spot size and 8 mm FWHM mini-SOBP, scan step sizes in the x , y and z directions were all selected as 2 mm. The least-squares optimization algorithm was used to calculate the physical dose weight matrices for all scan points [24]. The cost function χ^2can be defined as

$$\chi^2=\sum_{i=1}^{N_1}(P_i-D_i)^2, \tag{1}$$

where P_i is the prescribed dose to a dose grid point i, D_i is its calculated dose, and N_1 is the total number of dose grid points. The weight for an arbitrary pencil beam j after the k-th iteration can be calculated using

$$W_{j,k}=W_{j,k-1}\left[\left[\sum_{i=1}^{N_1}d_{i,j}^2\left(\frac{P_i}{D_i}\right)\right]\left(\sum_{i=1}^{N_1}d_{i,j}^2\right)^{-1}\right], \tag{2}$$

$$D_i=\sum_{j=1}^{N_2}W_{j,k-1}d_{i,j}, \tag{3}$$

where $d_{i,j}$ is the unweighted dose contribution of the beam j to the dose grid point i, which is obtained by MC simulation and N_2 is the number of scanned pencil beams. The physical dose prescribed to the target volume was 1 Gy and only uniform physical dose distribution across the target volume was considered in this study.

The dose homogeneity [25, 26] was calculated using:

$$H_{\rm d}=1-\frac{\sigma_{\rm d}}{\overline{D}}, \tag{4}$$

$$\sigma_{\rm d}=\sqrt{\frac{1}{N_1-1}\sum_{i=1}^{N_1}(D_i-\overline{D})^2}, \tag{5}$$

where $\overline{D}$ is the mean dose of the all dose grid points.

3 Results

3.1 Longitudinal beam widening

The pristine Bragg peaks of 180 MeV/u and 360 MeV/u carbon ions in water were widened to Gaussian-shaped distributions with a FWHM of about 8 mm (i.e. mini-SOBP) by the mini-RF mentioned in the section above. Figure 4 shows that the mini-SOBPs of 180 MeV/u and 360 MeV/u carbon ions in water were modulated to be Gaussian-shaped distributions with FWHMs of about 10.4 mm, 12.8 mm and 18. mm when tilting the mini-RF 30°, 45° and 60°, respectively. In other words, tilting mini-RF 30°, 45° and 60° increased the width of the original mini-SOBP by factors of 16%, 42% and 100%, respectively. Of course, the range of the carbon ions in water became shorter when tilting the mini-RF and thus the range-energy relationship for carbon ions passing through the mini-RF with different angle tilting was recalculated (Fig. 5).

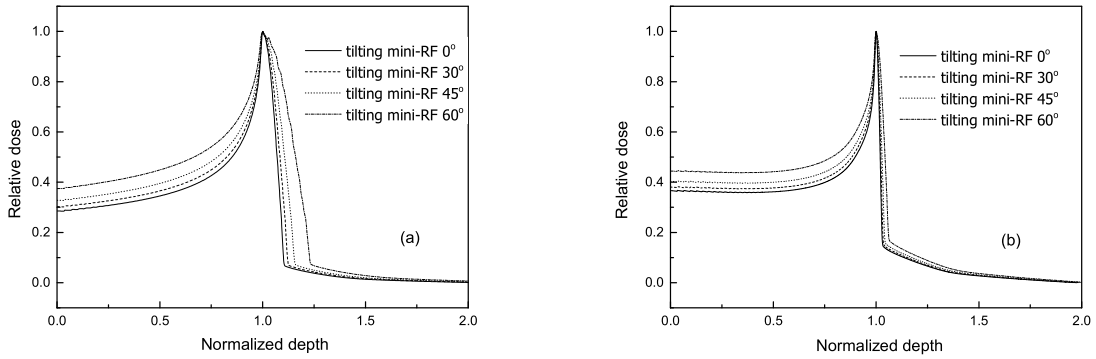

Fig. 4. Dose distributions in depth of water for carbon ion beams of 180 MeV/u (a) and 360 MeV/u (b) modulated by the mini-RF and tilting the mini-RF with different angles.

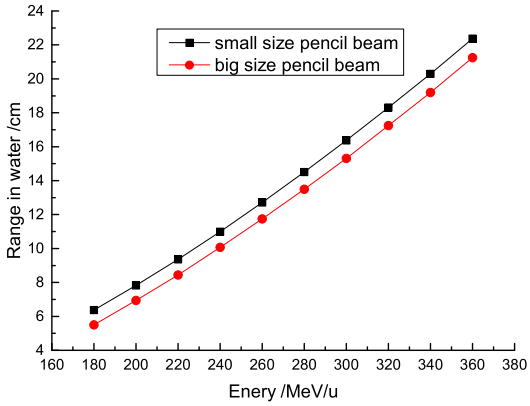

Fig. 5. (color online) Carbon ion range-energy relationships for small size pencil beams with 3 mm sigma spot size and 8 mm FWHM SOBP, and large size pencil beam with about 5 mm sigma spot size and 16 mm FWHM SOBP. The small size pencil beam means the pencil beam after passing through the mini-RF tilted at 0°. The large size pencil beam means the pencil beam after passing through the mini-RF tilted at 60° and a scatterer.

3.2 Lateral beam broadening

Tilting the mini-RF, which is 65 cm from the iso-center, by 30°, 45° and 60° could only broaden the lateral size of the beam spots slightly (no more than 20%), whereas inserting a tantalum scatterer of different thicknesses could enlarge the lateral size of the beam spots significantly (see Table 1). Table 2 presents the thicknesses of tantalum scatterer to enlarge the beam spot size (σ) from 3 mm to about 5 mm at the iso-center for carbon ions of different energies. To obtain the same beam spot size at the iso-center, the higher the pencil beam's energy, the thicker the tantalum scatterer was. The thickness of tantalum scatterer was no more than 0.4 mm for carbon ions with energies varying from 180 MeV/u to 360 MeV/u. Using almost the same thickness of Ta scatterer could enlarge the beam spots of the pencil beams with approximately equal energies to a similar size at the iso-center.

Table 1. Lateral sizes of the beam spots of 180 MeV/u and 360 MeV/u carbon ions under different conditions.

	180 MeV/u	360 MeV/u
tilting mini-RF 0°	2.99 mm	3.00 mm
tilting mini-RF 30°	3.23 mm	3.07 mm
tilting mini-RF 45°	3.41 mm	3.13 mm
tilting mini-RF 60°	3.60 mm	3.19 mm
0.15 mm thick Ta	5.41 mm	
0.4 mm thick Ta		4.81 mm

Table 2. Thickness of Ta scatterer for carbon ions with different energies.

energy/(MeV/u)	200	220	240	260	280	300	320	340
Ta thickness /mm	0.15	0.2	0.2	0.25	0.3	0.35	0.35	0.4
original σ at the iso-center /mm	3.00	3.00	3.00	3.00	3.00	3.00	3.00	3.00
σ at the iso-center /mm	5.06	5.18	4.92	5.01	5.07	5.11	4.93	4.96

3.3 Basic data for beam weight optimization

The basic data used in the beam weight optimization includes the range-energy relationships (Fig. 5), depth dose distributions (Fig. 6) and depth-sigma distribution (Fig. 7). The small size pencil beams with 3 mm sigma spot size and 8 mm FWHM SOBP pass the mini-RF tilted at 0°. The large size pencil beams with about 5 mm sigma spot size and 16 mm FWHM SOBP pass the mini-RF tilted at 60°and a scatterer. The thicknesses of scatterer were different for different energy carbon ions (Table 2).

3.4 Dose distributions optimized for beam deliveries under different conditions

Figures 8 and 9 show the optimized physical dose distributions for the three beam delivery modes. The dose homogeneities in the target volume were about 97.8%, 97.9%, 97.4% for spot-scanning beam delivery using the single large size pencil beams, single small size pencil beams, and laterally- and longitudinally-mixed size pencil beams, respectively. As shown in Fig. 8(d), the lateral dose penumbras at the depth of 10 cm in water for the mixed size spot-scanning and small size spot-scanning were both 4 mm, whereas the lateral dose penumbra at the depth of 10 cm in water for the large size spot-scanning was more than 5.8 mm. Figure 9(d) shows that the distal dose fall-off distances for the mixed size spot-scanning and small size spot-scanning were both 7.6 mm while the distal dose fall-off distance for the big size spot-scanning was about 10 mm. The mixed size spot-scanning mode could achieve a smaller lateral dose penumbra and distal dose fall-off distance than the large size spot-scanning.

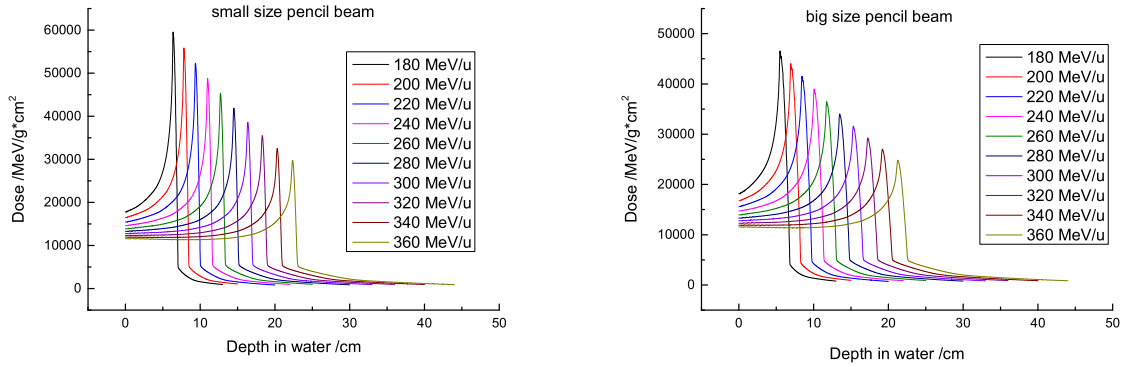

Fig. 6. (color online) Depth dose distributions for carbon ion pencil beams. The small size pencil beams have 3 mm sigma spot size and 8 mm FWHM mini-SOBP (left), and the large size pencil beams have about 5 mm sigma spot size and 16 mm FWHM mini-SOBP (right).

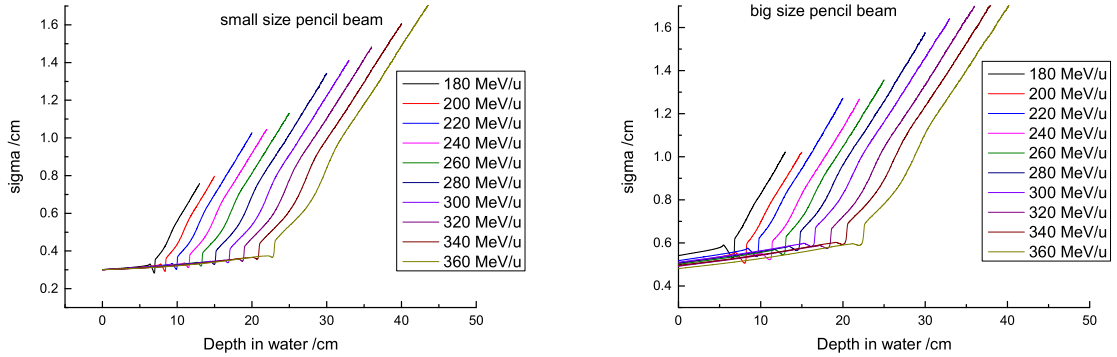

Fig. 7. (color online) Depth dependence of the lateral basic data (sigma value) for carbon ion pencil beams. The small size pencil beams have 3 mm sigma spot size and 8 mm FWHM mini-SOBP (left), and the large size pencil beams have about 5 mm sigma spot size and 16 mm FWHM mini-SOBP (right).

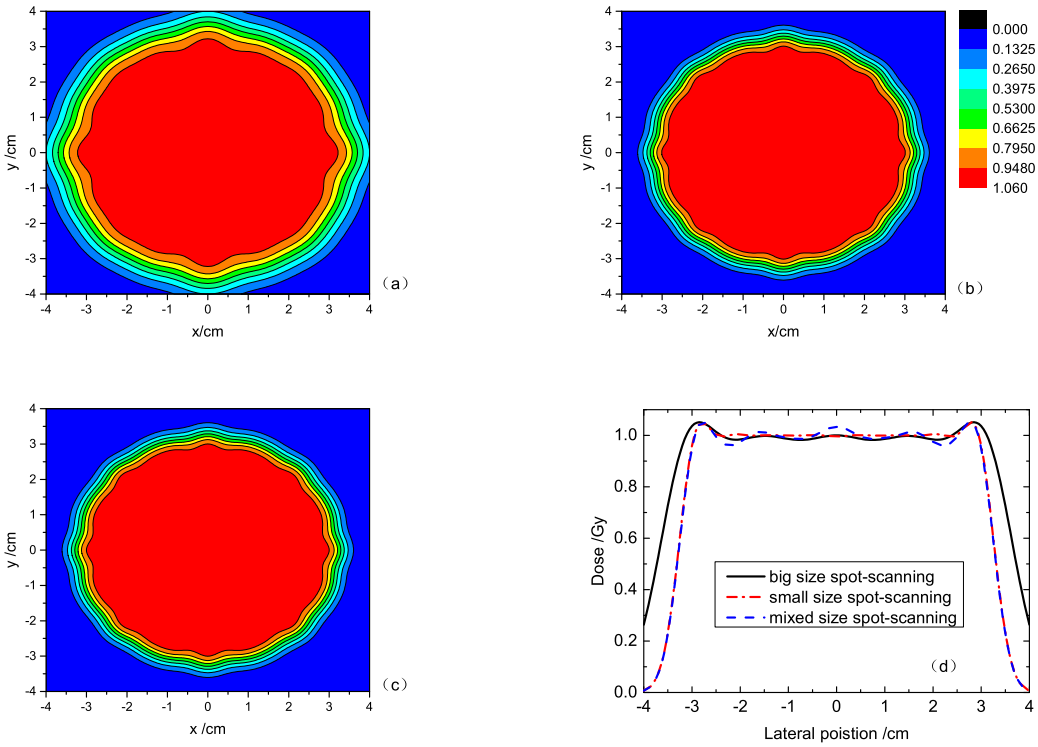

Fig. 8. (color online) Physical dose distributions for large size spot-scanning (a), small size spot-scanning (b), mixed size spot-scanning (c) and lateral dose penumbras at the middle iso-energy slice (10 cm depth in water) of the target volume (d).

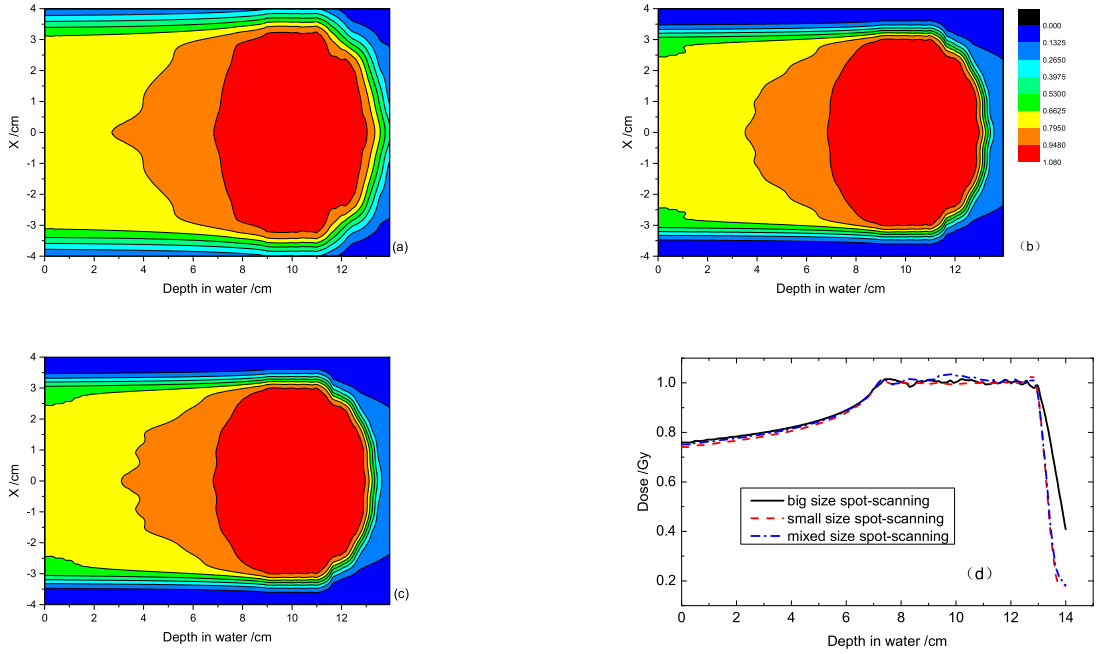

Fig. 9. (color online) Physical dose distributions for large size spot-scanning (a), small size spot-scanning (b), mixed size spot-scanning (c) and distal dose fall-off distances at the middle z-y plane (x=0 cm) of the target volume (d).

3.5 Issues related to dosimetry

Figure 10 shows the positions of scan points and corresponding particle numbers required for spot-scanning beam delivery with the single large size pencil beams, single small size pencil beams, and laterally- and longitudinally-mixed size pencil beams, respectively. The statistical results (Fig. 10(d)) indicates that the great majority of the scan points in the small size spot-scanning beam delivery were exposed to numbers of carbon ions of the order of magnitude of 10^5 while numbers of carbon ions of the order of magnitude of 10^6were mostly used in the cases of mixed size and big size spot-scanning modes. The numbers of scan points for the mixed size and large size spot-scanning beam deliveries were far less than those for the small size spot-scanning beam delivery. Consequently, if there were some errors in the number of carbon ions delivered due to the time delay of the interlock control system, this had less influence on the dose distribution in the target volume for the mixed size spot-scanning beam deliveries than for the small size spot-scanning beam delivery.

As shown in Fig. 11(a), in the case where the beam was not cut off in advance, i.e. the particle number threshold value was 0, the dose homogeneity in the target volume decreased sharply as the beam intensity increased. The dose homogeneities in the target volume for the mixed size and large size spot-scanning beam deliveries were better than 95% under the condition of all beam intensities and varied little as the beam intensity increased. But the dose homogeneity in the target volume for the small size spot-scanning beam delivery was better than 95% only when the beam intensity was below 1×10^7 pps. It is concluded that the particle number threshold value evaluated empirically is relevant to the beam intensity for the small size spot-scanning beam delivery. As shown in Fig. 11(b), when the beam intensity reached 3×10^7 pps, the dose homogeneities in the target volume for the mixed size and large size spot-scanning beam deliveries were better than 95% for all particle number threshold values, while those for the small size beam delivery were better than 95% only for a few particle number threshold values. The dose homogeneity in the target volume for the small size spot-scanning beam delivery was better than 95% only when the particle number threshold value changed from about 13000

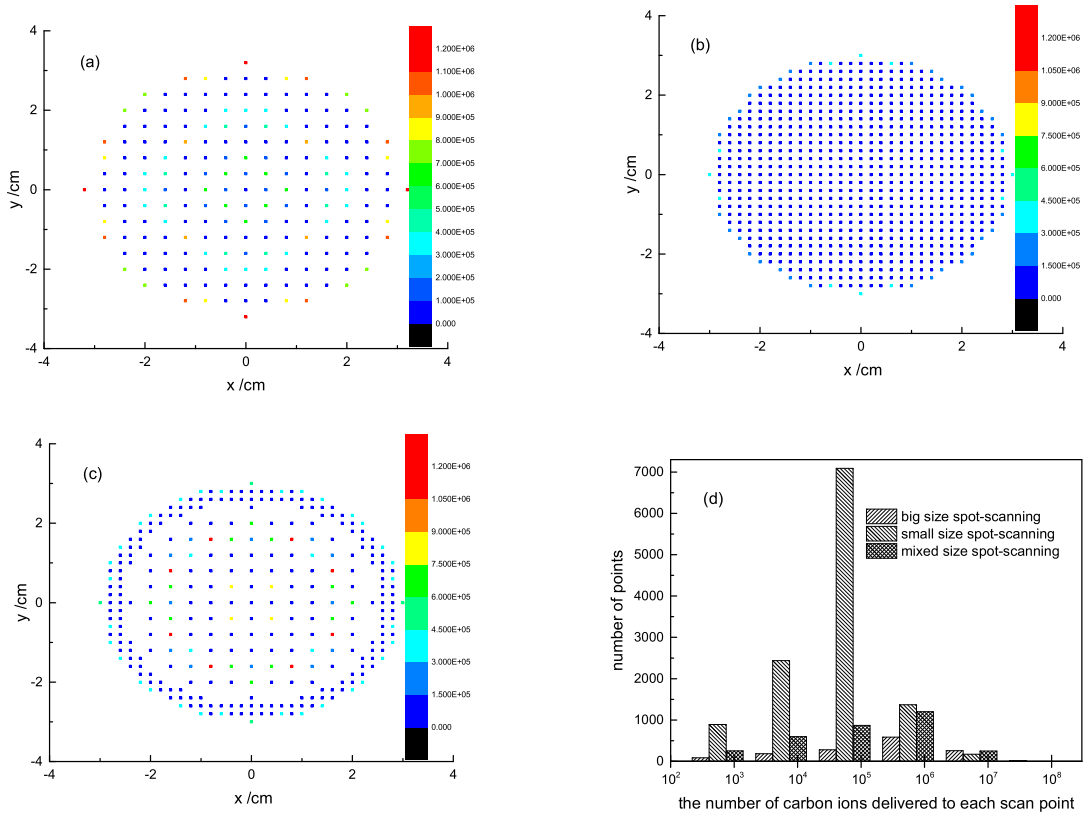

Fig. 10. (color online) Scan point position and number of carbon ions delivered to the middle energy slice in the target volume for the large size spot-scanning (a), small size spot-scanning (b), mixed size spot-scanning (c) and the statistics of the scan point numbers in the target volume under the three mode spot-scanning beam deliveries (d).

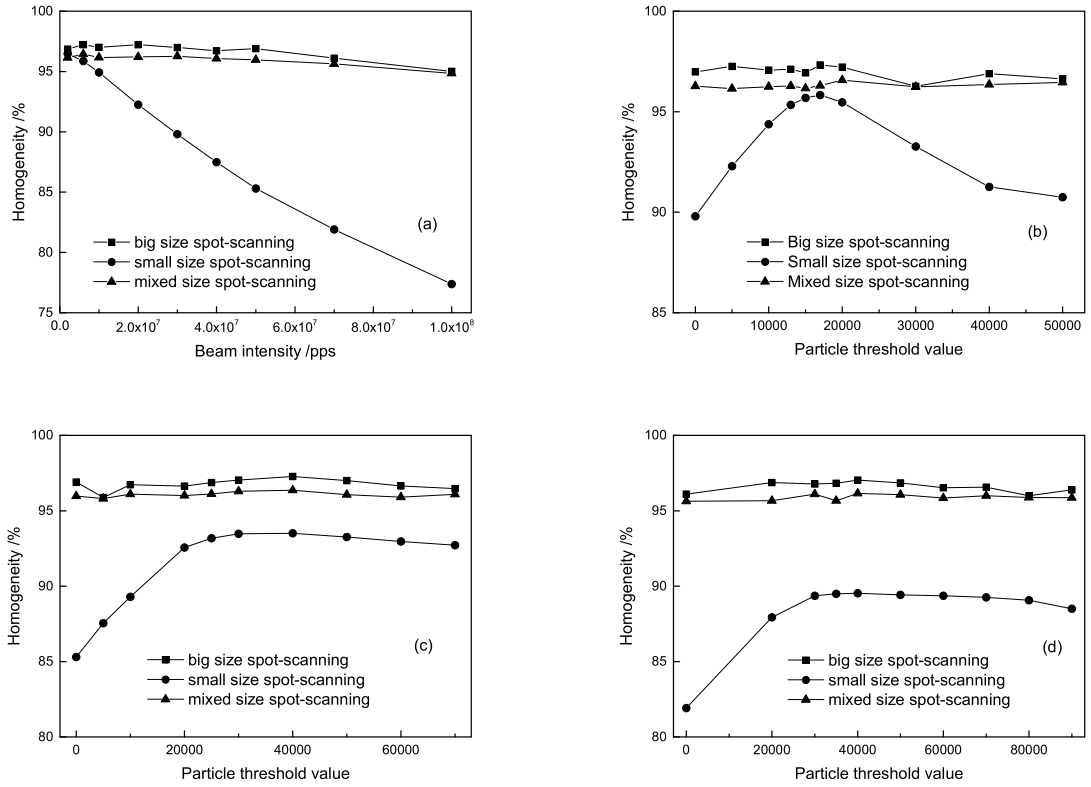

Fig. 11. Dose homogeneities for the three mode spot-scanning beam delivery (a) with particle number threshold value 0 under different beam intensities, with different particle number threshold values (b) under beam intensity of 3×10^7 pps, (c) under beam intensity of 5×10^7 pps, and (d) under beam intensity of 7×10^7 pps.

to about 20000. Figures 11(c) and 11(d) show that when the beam intensity reached 5×10^7 pps and 7×10^7 pps, the dose homogeneities in the target volume for the mixed size and large size spot-scanning beam deliveries were more than 95% for all particle number threshold values; the maximum homogeneity values 93.5% and 89.5% for the small size spot-scanning beam delivery under the beam intensities of 5×10^7 pps and 7×10^7 pps were worse than 95%. Obviously, the homogeneities in the target volume irradiated with the mixed size and large size methods were affected little by the particle number threshold value, while with the small size spot-scanning beam delivery it relied heavily on the particle number threshold value when the beam intensity was smaller and could not reach 95%, which is required in dosimetry, when the beam intensity increased.

4 Discussion

The dose penumbra and fall-off distance for the mixed size spot-scanning beam delivery were definitely smaller than those for the big size spot-scanning beam delivery. In view of protecting the healthy tissue and OAR near the target volume, the mixed size method was superior to the large size one. The dose homogeneity in the target volume for the mixed size spot-scanning beam delivery was affected little by the beam-off delay and was more robust than the small size spot-scanning beam delivery. Without controlling the accelerator, switching between two size pencil beams in the mixed size spot-scanning beam delivery was through tilting the mini-RF and inserting the Ta scatterer. This pencil beam switching method is convenient and fast. Overall, the mixed size spot-scanning beam delivery is a more ideal method than the traditional single size spot-scanning method.

Biological effectiveness was not considered in this study, but will be investigated in the near future. Once Ta as the scatterer is involved, secondary particles, especially neutrons, need to be considered further. The mixed size spot-scanning beam delivery as well as the pencil beam size variation method laterally and longitudinally remains to be verified experimentally.

5 Conclusions

The simulation studies have shown that the spot-scanning method using laterally- and longitudinally-mixed size pencil beams achieves the desired effects such

as small dose penumbra, small distal dose fall-off distance, and robust dose homogeneity for carbon ions. In addition, this kind of spot-scanning beam delivery is characterized by easy alteration of the lateral and longitudinal sizes of the pencil beam. Without controlling the accelerator, the lateral size of the pencil beam was broadened by means of inserting a scatterer, and the mini-SOBP width of the pencil beam was widened longitudinally by tilting a mini-RF. Thus, the new spot-scanning beam delivery with laterally- and longitudinally-mixed size pencil beams is promising for application to heavy ion radiotherapy.

References

1 T. Kanai, K. Kawachi, Y. Kumamoto et al, Med. Phys., **7**(4): 365–369 (1980)
2 T. Haberer, W. Becher, and D. Schardt, Nucl. Instrum. Methods Phys. Res. Sect. A, **330**(1-2): 296–305 (1993)
3 J. H. Kang, J. J. Wilkens, and U. Oelfke, Med. Phys., **34**(9): 3457–3464 (2007)
4 H. Tsujii, T. Kamada, T. Shirai et al, *Carbon-Ion Radiotherapy* (Germany: Springer, 2014), p.58–60
5 Q. Li, X. G. Liu, Z. Y. Dai et al, edited by W. Liu et al, *American Institute of Physics Conference Series* (AIP Publishing, 2013), p.174–178
6 Z. Y. Dai, Q. Li, and X. G. Liu, Chin. Phys. C, **36**(8): 784–791 (2012)
7 T. Inaniwa, T. Furukawa, and T. Tomitani, Med. Phys., **34**(8): 3302–3311 (2007)
8 T. Furukawa, K. Noda, Nucl. Instrum. Methods Phys. Res. Sect. A, **489**(1-3): 59–67 (2002)
9 T. Furukawa, K. Noda, E. Urakabe, Nucl. Instrum. Methods Phys. Res. Sect. A, **503**(3): 485–495 (2003)
10 J. H. Kang, *Optimization of Scanning Parameters in Intensity Modulated Proton Therapy*, Ph.D.Thesis (Germany: the Ruperto-Carola University of Heidelberg, 2008)
11 S. Fujitaka, T. Takayanagi, and R. Fujimoto, Phys. Med. Biol., **54**(10): 3101–3111 (2009)
12 T. Nakagawa, K. Yoda, Med. Phys., **27**(4): 712–715 (2000)
13 J. C. Yang, J. Shi, and W. P. Chai, Nucl. Instrum. Methods Phys. Res. Sect. A, **756**: 19–22 (2014)
14 J. Shi, J. C. Yang, J. W. Xia et al, Nucl. Instrum. Methods Phys. Res. Sect. A, **714**: 105–109 (2013)
15 N. Bassler, Armin Luhr, D. C. Hansen et al, SHIELD-HIT12A-User's Guide (2016)
16 N. Bassler, D. C. Hansen, A. Luhr et al, *Journal of Physics: Conference Series* (IOP Publishing, 2014), 012004
17 D. C. Hansen, A. Luhr, and R. Herrmann, International Journal of Radiation Biology, **88**(1-2): 195–199 (2012)
18 Y. L. Yan, X. G. Liu et al, Nuclear Physics Review, **33**(1): 105–111 (2016)(in chinese)
19 M. Torikoshi, S. Minohara, N. Kanematsu et al, Journal of Radiation Research, **48**(Suppl A): A15–A25 (2007)
20 T. Himukai, T. Furukawa, and E. Takeshita, Nucl. Instrum. Methods Phys. Res. Sect. B, **269**(24): 2891–2894 (2011)
21 B. Schaffner, T. Kanai, and Y. Futami, Med. Phys., **27**(4): 716–724 (2000)
22 U. Weber, G. Kraft, Phys. Med. Biol., **44**(11): 2765–2775 (1999)
23 M. Kramer, O. Jakel, and T. Haberer, Phys. Med. Biol. Printed in the UK, **45**(11): 3299–3317 (2000)
24 A. Lomax, Phys. Med. Biol., **44**(1): 185–205 (1999)
25 M. H Phillips, E. Pedroni, H. Blattmann et al, Phys. Med. Bid. Printed in the UK, **37**(1): 223–234 (1992)
26 Christoph Bert, Sven O Grozinger, and Eike Rietzel, Phys. Med. Biol., **53**(9): 2253–2265 (2008)